The Astrophysical Journal, 813:36 (8pp), 2015 November 1 doi:10.1088/0004-637X/813/1/36

ON THE [C II]–SFR RELATION IN HIGH REDSHIFT GALAXIES

L. Vallini[1,2], S. Gallerani[3], A. Ferrara[3,4], A. Pallottini[3], and B. Yue[3]
[1] Dipartimento di Fisica e Astronomia, Universitá di Bologna, Viale Berti Pichat 6/2, I-40127 Bologna, Italy
[2] Scuola Normale Superiore, Pisa, Italy
[3] Scuola Normale Superiore, Piazza dei Cavalieri 7, I-56126 Pisa, Italy
[4] Kavli IPMU (WPI), Todai Institutes for Advanced Study, the University of Tokyo, Japan
Received 2015 June 25; accepted 2015 September 2; published 2015 October 27

ABSTRACT

After two Atacama Large Millimeter/submillimeter Array (ALMA) observing cycles, only a handful of [C II] 158 μm emission line searches in $z > 6$ galaxies have reported a positive detection, questioning the applicability of the local [C II]–star formation rate (SFR) relation to high-z systems. To investigate this issue we use the Vallini et al. (V13) model,based on high-resolution, radiative transfer cosmological simulations to predict the [C II] emission from the interstellar medium of a $z \approx 7$ (halo mass $M_{\rm h} = 1.17 \times 10^{11}\,M_{\odot}$) galaxy. We improve the V13 model by including (a) a physically motivated metallicity (Z) distribution of the gas, (b) the contribution of photodissociation regions (PDRs), and (c) the effects of cosmic microwave background (CMB) on the [C II] line luminosity. We study the relative contribution of diffuse neutral gas to the total [C II] emission ($F_{\rm diff}/F_{\rm tot}$) for different SFR and Z values. We find that the [C II] emission arises predominantly from PDRs: regardless of the galaxy properties, $F_{\rm diff}/F_{\rm tot} \leqslant 10\%$, since at these early epochs the CMB temperature approaches the spin temperature of the [C II] transition in the cold neutral medium ($T_{\rm CMB} \sim T_s^{\rm CNM} \sim 20$ K). Our model predicts a high-z [C II]–SFR relation, consistent with observations of local dwarf galaxies ($0.02 < Z/Z_{\odot} < 0.5$). The [C II] deficit suggested by actual data ($L_{\rm CII} < 2.0 \times 10^7\,L_{\odot}$ in BDF3299 at $z \approx 7.1$) if confirmed by deeper ALMA observations, can be ascribed to negative stellar feedback disrupting molecular clouds around star formation sites. The deviation from the local [C II]–SFR would then imply a modified Kennicutt–Schmidt relation in $z > 6$ galaxies. Alternatively/in addition, the deficit might be explained by low gas metallicities ($Z < 0.1\,Z_{\odot}$).

Key words: cosmology: observations – cosmology: theory – galaxies: high-redshift – galaxies: ISM – line: formation – submillimeter: ISM

1. INTRODUCTION

The study and characterization of the interstellar medium (ISM) of galaxies that formed in the early universe is entering a golden era thanks to the unprecedented capabilities of the Atacama Large Millimeter/submillimeter Array (ALMA). In particular, the 158 μm emission line due to the $^2P_{3/2} \rightarrow {}^2P_{1/2}$ fine-structure transition of ionized carbon ([C II]), being the dominant coolant of the neutral diffuse ISM (Wolfire et al. 2003), is by far the brightest line in the far-infrared band (Stacey et al. 1991). In addition to the diffuse neutral gas, the [C II] line can be excited in other components of the ISM such as high density photodissociation regions (PDRs), and in the diffuse ionized gas, where the main drivers of [C II] emissivity are collisions with free e^-. Although precisely assessing the relative contribution of the various gas phases to the total line emission might be difficult, the [C II] line remains an exquisite proxy for characterizing the ISM of galaxies that formed during the Epoch of Reionization (EoR; $z \approx$ 6–7; e.g., Carilli & Walter 2013). Before the ALMA advent, the [C II] line from $z > 4$ was solely detected in galaxies with extreme star formation rates (SFRs; $\approx$1000 $M_{\odot}$ yr^{-1}; e.g., Cox et al. 2011; Carilli et al. 2013; Carniani et al. 2013; De Breuck et al. 2014), or in those hosting active galactic nuclei (AGNs; e.g., Maiolino et al. 2005; Gallerani et al. 2012; Venemans et al. 2012; Cicone et al. 2015).

In the first years of ALMA operations, the [C II] emission line has been detected in a handful of galaxies with modest SFRs (50–300 $M_{\odot}$ yr^{-1}) at $z \approx 4.5$, i.e., approximately 400 Myr after the end of the EoR (Carilli et al. 2013; Carniani et al. 2013; Riechers et al. 2014; Williams et al. 2014). Vice versa, other tentative searches of this line have failed in normal star-forming galaxies (SFR $\approx$10 $M_{\odot}$ yr^{-1}) at the end of the EoR ($z \gtrsim 6$; e.g., Walter et al. 2012; Kanekar et al. 2013; Ouchi et al. 2013; González-López et al. 2014; Ota et al. 2014; Schaerer et al. 2015). These early results seemed to be at odds with the correlation between the intensity of the [C II] line and the SFR observed in local galaxies (De Looze et al. 2011, 2014), thus questioning its applicability to sources at $z \gtrsim 6$. Only very recently, three different ALMA campaigns targeting $z \approx$ 5–7 Lyman alpha emitters (LAEs) and Lyman break galaxies (LBGs) have yielded [C II] detections: Maiolino et al. (2015) in the vicinity of BDF3299, a LAE at $z \approx 7.1$, Capak et al. (2015) in a sample of LAEs at $5.1 < z < 5.7$, and Willott et al. (2015) in two luminous LBGs at $z \approx 6$, being in agreement with the [C II] luminosity expected from lower-z observations in star-forming galaxies.

In the nearby universe, the [C II]–SFR relation holds for a wide range of galaxy types, ranging from metal-poor dwarf galaxies, to starbursts, ultra-luminous infrared galaxies, and AGN-hosting galaxies (Boselli et al. 2002; De Looze et al. 2011, 2014; Sargsyan et al. 2012; Pineda et al. 2014; Herrera-Camus et al. 2015). The [C II] emission from PDRs is primarily due to the far-ultraviolet (FUV) radiation produced by OB stars that form in the vicinity of the PDRs (Hollenbach & Tielens 1999). The relation between SFRs and the [C II] luminosity in the neutral diffuse gas is more subtle. On one hand, the [C II] emissivity is proportional to the gas heating due to the photoelectric effect on dust grains, namely to the intensity of the FUV radiation (Wolfire et al. 2003; Herrera-Camus et al. 2015). On the other hand, an increasing FUV radiation reduces the relative abundance of the cold neutral

medium (CNM) with respect to the warm neutral medium (WNM), thus reducing the [C II] luminosity (Vallini et al. 2013). Observational studies have found that in the plane of the Galaxy, the [C II] emission is mostly associated with dense PDRs (Pineda et al. 2013). On the contrary, in low-metallicity local dwarf galaxies (e.g., Haro 11, Cormier et al. 2012), nearby galaxies (e.g., M51 and M31, Kramer et al. 2013; Parkin et al. 2013; Kapala et al. 2015) and the outskirts of the Milky Way (Langer et al. 2014) the PDR contribution can be as small as ≈10%. The [C II]–SFR relation in these cases is shallower than that of starburst galaxies (De Looze et al. 2014).

From a theoretical point of view the intensity of the [C II] line from high-z galaxies has been computed both through numerical simulations (e.g., Nagamine et al. 2006) and semi-analytical models (e.g., Gong et al. 2012; Muñoz & Furlanetto 2014; Popping et al. 2014). Recently Olsen et al. (2015) presented a multi-phased ISM model consisting of molecular clouds (MCs) embedded within a CNM of atomic gas, and hot, partly ionized gas. The model, applied on top of a cosmological smoothed-particle hydrodynamics (SPH) simulation of massive star-forming galaxies on the main sequence at $z = 2$, self-consistently calculates the relative contribution of the various phases to the [C II] emission.

In the previous paper of this series Vallini et al. (2013; hereafter, V13) computed the [C II] emission arising from the neutral diffuse gas of a single prototypical high-z ($z \approx 6.6$) galaxy, extracted from an SPH cosmological simulation, further implemented with a radiative transfer (RT) calculation. This is crucial for modeling the intensity of the galaxy internal UV field and the consequent gas ionization structure. The calculation of the [C II] emission is performed thanks to a sub-grid model describing the thermal equilibrium of the CNM and WNM as a function of the FUV radiation field intensity within the galaxy. The spatial resolution (≈60 pc) allows us to properly describe the ISM small-scale density structure. Here we present an updated version of the V13 model that allows us to also compute the [C II] emission arising from the clumpy molecular gas, and the effect of the increased cosmic microwave background (CMB) temperature on the [C II] observability. The aim is to finally assess whether the local [C II]–SFR relation holds at high-z, and what we can learn from any deviation from it.

2. MODELING [C II] EMISSION

In this section, we first summarize the main characteristics of the V13 model, referring the interested reader to V13 for further details. Next, we describe the additional features implemented by this work.

2.1. The V13 Model

We run GADGET-2 (Springel 2005) cosmological SPH hydrodynamic simulations of a $(10h^{-1}\,\mathrm{Mpc})^3$ comoving volume with a mass resolution of 1.32 $(6.68) \times 10^5\,M_\odot$ for baryons (dark matter). We take a snapshot at redshift $z = 6.6$, identify the most massive halo (total mass $M_\mathrm{h} = 1.17 \times 10^{11}\,M_\odot$, $r_\mathrm{vir} \approx 20$ kpc), and select a $(0.625h^{-1}\,\mathrm{Mpc})^3$ comoving volume around the center of the halo. We post-process our simulations with the UV RT code LICORICE. Gas properties are resolved on a fixed grid with a resolution of ∼60 pc. We complement the simulation with a sub-grid model that takes into account the cooling and heating processes that produce a multi-phase thermal ISM structure (Wolfire et al. 1995, 2003). According to this model, the neutral gas in the ISM is constituted by a two-phase medium in which the CNM and the WNM are in pressure equilibrium. The relative abundance of these two components depends on (i) the gas metallicity, Z, determining the coolants abundance, and (ii) the FUV flux, G_0, in the Habing (6–13.6 eV) band, controlling the photoelectric heating produced by dust grains. The value of G_0 scales with SFR and is calculated as

$$G_0(\boldsymbol{r}, \mathrm{SFR}) = \mathrm{SFR} \times \Sigma_{i=1}^{n_*} \frac{\int_{6\,\mathrm{eV}}^{13.6\,\mathrm{eV}} l_{\nu,i}\, d\nu}{4\pi\,|\boldsymbol{r} - \boldsymbol{r}_i|^2}, \quad (1)$$

where n_* is the number of sources, $\boldsymbol{r}_i$ is the positions, and $l_{\nu,i}$ is the monochromatic luminosity per source. We compute $l_{\nu,i}$ by using the STARBURST99 template of Leitherer et al. (1999), assuming continuous star formation (SF), an age of 10 Myr for the stellar population,[5] and accordingly setting the metallicity to the cell value (see Section 2.2). In this work we explore the range $\mathrm{SFR} = [0.1\text{–}100]\,M_\odot\,\mathrm{yr}^{-1}$. For each value of the SFR and metallicity we run the V13 sub-grid model, computing the expected distribution of the cold and warm diffuse gas within the galaxy.

We calculate the [C II] emissivity through Equation (3) of V13. We note that this equation is valid under the assumption that the density of the colliding species (electrons and hydrogen atoms) is much lower than their corresponding critical densities[6] and that no external radiation field is present. While the first assumption is justified by the fact that in our simulation $n_e \ll n_\mathrm{crit}^e = 8\,\mathrm{cm}^{-3}$ and $n_\mathrm{H} \ll 3000\,\mathrm{cm}^{-3}$, in Section 2.3 we investigate whether the CMB may affect the intensity of the [C II] emission. As pointed out in V13, the CNM accounts for ≈95% of the total [C II] emission arising from the diffuse neutral medium. Given this result, we refer to the diffuse medium as CNM.

2.2. Metallicity

The V13 model assumes that metals are uniformly distributed within the galaxy. Hereafter, we refer to models with uniform metallicity distributions as[7] "C-models." In this work, we also consider the possibility that the distribution of metals follows the density distribution by relating Z to the baryonic overdensity of each cell $\Delta \equiv \rho_\mathrm{gas}/\rho_\mathrm{c}(z)$, where ρ_gas is the gas density in the cell and $\rho_\mathrm{c}(z)$ is the critical density at redshift z. This is in agreement with the parameterization adopted by Keating et al. (2014) to describe the circumgalactic medium of high-z galaxies, and with the results presented in Pallottini et al. (2014a, P14), which have been applied to our galaxy.

[5] We keep fixed the original assumption of V13, in which a continuous SF with an age of $t_* = 10$ Myr for the stellar population was based on the Himiko spectral energy distribution fitting presented in Ouchi et al. (2009, 2013). This scenario has recently been confirmed by Zabl et al. (2015) and Schaerer et al. (2015); when adopting continuous/exponential rising (declining) SF histories for Himiko, one obtains an age of the stellar population in the ranges $t_* = 1$–35 Myr (Zabl et al. 2015) and $t_* = 10$–40 Myr (Schaerer et al. 2015).

[6] The critical density for collision with neutral hydrogen atoms (or with e^-) has been computed at $T = 100$ K, a value consistent with the CNM temperature.

[7] For example, we indicate with C02 a model in which a uniform $Z = 0.2\,Z_\odot$ is imposed.

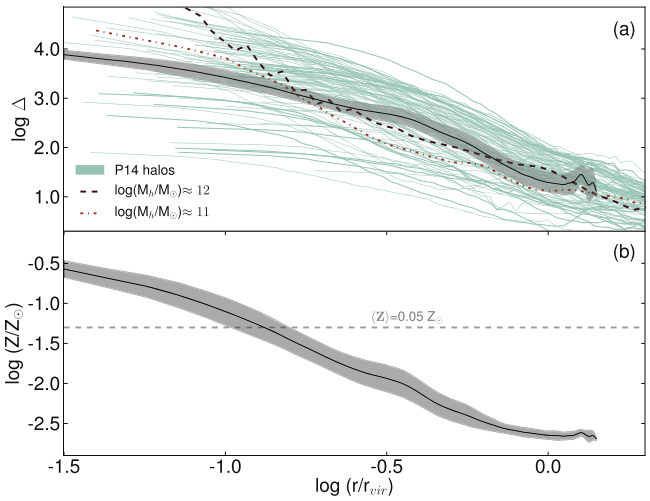

Figure 1. Panel (a): the black solid line and the gray shaded region represent the radial profile of the baryonic overdensity (Δ) and its rms fluctuation for our simulated galaxy. The distance is rescaled with the virial radius of the galaxy. With light cyan lines we plot the mean profiles for the ∼100 galaxies in the Pallottini et al. (2014a, P14) simulation (see also Figure 1 in Pallottini et al. 2014b). Using dashed/dotted–dashed lines we highlight the two most massive P14 galaxies. Such galaxies are hosted in dark matter halos with masses $\log(M_{\rm h}/M_\odot) \approx 12$ and $\log(M_{\rm h}/M_\odot) \approx 11$, respectively, comparable to the mass of the galaxy adopted in this work ($\log(M_{\rm h}/M_\odot) \approx 11.1$). Panel (b): metallicity (Z) radial profile for the P005' model. For the P005 model, Z is calculated using the density of our simulated galaxy and rescaling the Z–Δ relation found in P14. The relation is rescaled so that the mean metallicity of the galaxy is $\langle Z\rangle = 0.05\,Z_\odot$ (gray dashed line). Note that $\langle Z\rangle$ is calculated considering only those cells whose baryonic overdensities are $\Delta > 200$, i.e., up to $r/r_{\rm vir} \approx 0.5$. The MCs are on average clusterized near the center, and this affects their mean metallicity.

P14 use a customized version of the adaptive mesh refinement code RAMSES (Teyssier 2002) in order to investigate the metal enrichment of high-z galaxies. In P14 SF is included via sub-grid prescriptions, and supernovae feedback is accounted for by implementing a metal-dependent parameterization of stellar yields and return fractions based on population-synthesized models. The P14 galaxy sample reproduces the observed cosmic SFR (Bouwens et al. 2012; Zheng et al. 2012) and stellar mass densities' (González et al. 2011) evolutions in the redshift range $4 \leqslant z \lesssim 10$. In the upper panel of Figure 1 we plot the radial profile of the baryonic overdensity (Δ) and its rms fluctuation of our simulated galaxy. We test the profile with a sample of ∼100 galaxies extracted from P14 (see also Pallottini et al. 2014b, in particular the upper panel of their Figure 1). Among the P14 galaxies, using solid dashed/dotted–dashed lines we highlight two galaxies hosted in dark matter halos with masses $\log(M_{\rm h}/M_\odot) \approx 12$ and $\log(M_{\rm h}/M_\odot) \approx 11$, respectively. This is comparable to the dark matter halo mass of the galaxy adopted in this work ($\log(M_{\rm h}/M_\odot) \approx 11.1$).

In particular, P14 found a tight correlation between Z and Δ for $\log\Delta \gtrsim 2$, namely for overdensities typical of galaxy outskirts/ISM. While in the intergalactic medium ($\log\Delta \leqslant 2.3$) the metallicity is only weakly correlated with Δ, in the ISM ($2.3 < \log\Delta < 4.5$) the Z–Δ relation is tight. This is due to the fact that the most overdense regions denote the location in which stars form, and are therefore more efficiently polluted with metals. We fit the Z–Δ relation provided in their paper and we normalize the relation to the mean metallicity $\langle Z\rangle$ over the galaxy, i.e., over those cells whose overdensity is $\Delta > 200$. Hereafter, we refer to models that take into account this Z–Δ relation as "P-models." The density-dependent metallicity case with $\langle Z\rangle = 0.05 Z_\odot$ is called P005, and the profile is shown in the (b) panel of Figure 1.

2.3. MCs and PDRs

Beside the emission arising from the diffuse neutral medium, the [C II] line can be excited in the so-called PDRs (Tielens & Hollenbach 1985; Hollenbach & Tielens 1999) around MCs. To establish whether the gas in a cell becomes gravitationally bound, we apply the Jeans instability criterion. We define *molecular cells* as those satisfying the following condition: $M_{\rm cell} > M_{\rm J}(T_{\rm CMB}, n_{\rm cell})$, where $M_{\rm cell}$ is the mass of the gas in the cell, $M_{\rm J}$ is the Jeans mass at the CMB temperature ($T_{\rm CMB}$) at $z = 6.6$, and at the density of the gas in the simulation cell ($n_{\rm cell}$). As a caveat we note that it is possible that other processes such as cosmic ray heating (e.g., Papadopoulos 2010) can increase the temperature above the CMB floor, even at $z \approx 6$. By applying this prescription, we find that the total mass of molecular hydrogen in the simulated galaxy is $M_{\rm H_2} = 3.9\times10^8\,M_\odot$, consistent with previous theoretical estimates ($M_{\rm H_2} = 2.5\times10^8\,M_\odot$, Vallini et al. 2012) and observational constraints ($M_{\rm H_2} < 4.9\times10^9\,M_\odot$, Wagg et al. 2009) on $z \approx 7$ LAEs.

Since we find that on average the simulation cells contain a molecular hydrogen mass $\langle M_{\rm H_2}^{\rm cell}\rangle \sim 3\times10^3\,M_\odot$, we consider each molecular cell as a giant molecular cloud (GMC; $M_{\rm GMC} = 10^3$–$10^6\,M_\odot$, Murray 2011). The properties of GMCs are controlled by a turbulent and highly supersonic velocity field that causes isothermal shock waves (Padoan 1995; Ostriker et al. 2001; Padoan et al. 2014, p. 77). The problem of turbulent fragmentation of MCs can be treated analytically (e.g., Krumholz & McKee 2005; Hennebelle & Chabrier 2011, 2013; Padoan & Nordlund 2011) or numerically (e.g., Vazquez-Semadeni 1994; Kim & Ostriker 2002; Kim et al. 2003; Wada 2008; Tasker & Tan 2009). Analytical models as well as numerical simulations show that the distribution of the gas density ($n_{\rm cl}$) in an isothermal, non self-gravitating, turbulent medium follows a log-normal distribution (Padoan 1995; Padoan & Nordlund 2011):

$$p(\ln x)d\ln x = \frac{1}{\left(2\pi\sigma^2\right)^{1/2}}\exp\left[-\frac{1}{2}\left(\frac{\ln x - \overline{\ln x}}{\sigma}\right)^2\right], \quad (2)$$

where $x = n_{\rm cl}/\overline{n_{\rm cl}}$, $\overline{n}_{\rm cl} \simeq n_0\,\mathcal{M}^2$, n_0 is the average number density of the CNM ($n_0 = 50\,{\rm cm}^{-3}$, see V13), $\mathcal{M} = 10$ is the Mach number value suggested by Kainulainen & Tan (2013), and the turbulent velocity dispersion is given by $\sigma = \sqrt{\ln[1+(\mathcal{M}\beta^2)]}$, with $\beta = 0.5$ and $\overline{\ln x} = -0.5\sigma^2$. If we assume that each GMC in our simulation is composed of a set of clumps, we can compute the densities $n_{\rm cl}$ of each clump by adopting an iterative approach that consists of the following steps.

1. Select $n_{\rm cl}$ by sampling the density distribution (Equation (2)).
2. Set the clump radius equal to the Jeans length $r_{\rm cl} = \lambda_{\rm J}(T_{\rm CMB}, n_{\rm cl})$.
3. Calculate the clump mass $M_{\rm cl} = (8\pi/3)m_{\rm H}n_{\rm cl}r_{\rm cl}^3$.
4. If $M_{\rm cl} < M_{\rm cell}$, calculate the residual mass in the cell $M_{\rm cel}^{\rm new} = M_{\rm cell} - M_{\rm cl}$; go to step 1.

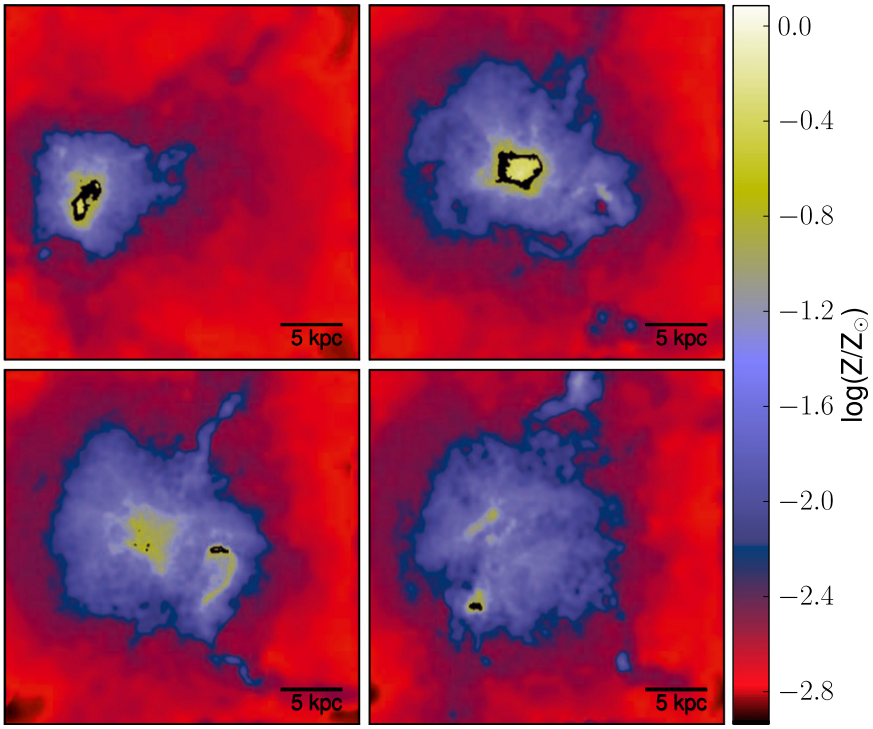

Figure 2. Slices of thickness 57 pc cut through the simulated galaxy for the P005 model showing the metallicity distribution (color scale) and molecular clouds (black regions). Note that the metallicity of the overdense regions in which MCs reside is greater than the mean value $\langle Z\rangle = 0.05\ Z_{\odot}$.

5. If $M_{\rm cl} > M_{\rm cell}$, reject the density sampled and assume $M_{\rm cl} = M_{\rm cell}$. Calculate $r_{\rm cl}$ as in step 2 and use it to derive the resulting clump density.

Through this procedure, we find that the MCs in the simulations are characterized by the following properties: $\langle \log(n_{\rm cl}/{\rm cm}^{-3})\rangle = 2.9 \pm 0.4$, $\langle M_{\rm cl}\rangle = 50 \pm 20\ M_{\odot}$ and radius $\langle r_{\rm cl}\rangle = 0.7 \pm 0.3$ pc.

In Figure 2, we show four 57 pc-thick slices of the simulated box showing the metallicity distribution and MCs (black regions) for the P005 model. By inspecting the maps shown in the figure we note that molecular cells reside in highly overdense regions mainly clustered at the center of the galaxy. The molecular cells are located predominantly in the innermost region of the galaxy ($d_{\rm MCs} \approx 1$ kpc) and have $Z \approx 0.2\,Z_{\odot}$, whereas the mean metallicity over the galaxy is $\langle Z\rangle = 0.05\ Z_{\odot}$. This implies that any line arising from the PDRs would provide an upper limit on the mean metallicity of the galaxy. Finally, to calculate the [C II] emission from PDRs, we couple our simulation with `UCL_PDR` (Bell et al. 2005, 2007; Bayet et al. 2009), a PDR code that allows us to derive the [C II] emissivity as a function of the intensity of the FUV radiation field (G_0, Section 2.1), metallicity (Z, Section 2.2), and molecular gas density ($n_{\rm cl}$, Section 2.3).

2.4. CMB Effects on [C II] Emission

Since the CMB sets the minimum temperature of the ISM to $T_{\rm CMB} = T^0_{\rm CMB}(1+z)$, at high z it represents a strong background against which the line fluxes are detected (e.g., da Cunha et al. 2013). The contrast of the cloud emission against the CMB radiation is given by the following relation:

$$\Delta I_{\nu} = \left[B_{\nu}(T_s) - B_{\nu}(T_{\rm CMB})\right]\left(1 - e^{-\tau_{\nu}}\right), \quad (3)$$

where T_s is the excitation (or spin) temperature. If we assume that the [C II] line is optically thin in the submillimeter, i.e., $e^{-\tau_{\nu}} \approx 1 - \tau_{\nu}$, the ratio ($(1+z)F_{\nu} \sim I_{\nu}/d_L^2$)) between the flux observed against the CMB and the intrinsic flux emitted by the cloud is (see also da Cunha et al. 2013)

$$\zeta \equiv \frac{F_{\nu}^{\rm ag}}{F_{\nu}^{\rm int}} = \frac{\left[B_{\nu}(T_s) - B_{\nu}(T_{\rm CMB})\right]\tau_{\nu}}{B_{\nu}(T_s)\tau_{\nu}} = 1 - \frac{B_{\nu}(T_{\rm CMB})}{B_{\nu}(T_s)}. \quad (4)$$

Equation (4) clearly shows that as the $T_{\rm CMB}$ approaches T_s the observed flux tends to be zero. The ratio of the population of the upper ($^2P_{3/2}$, labeled with u) and lower ($^2P_{1/2}$, labeled with l) levels of the [C II] 158 μm transition formally defines the spin temperature:

$$\frac{n_u}{n_l} = \frac{B_{lu}I_{\nu} + n_e C^e_{lu} + n_{\rm H} C^{\rm H}_{lu}}{B_{ul}I_{\nu} + A_{ul} + n_e C^e_{ul} + n_{\rm H} C^{\rm H}_{ul}} \equiv \frac{g_u}{g_l} e^{-T_*/T_s}, \quad (5)$$

where A_{ul} is the Einstein coefficient for spontaneous emission, B_{ul} (B_{lu}) is the stimulated emission (absorption) coefficient, C^e_{lu} ($C^{\rm H}_{lu}$) is the collisional excitation rate for collision with e^- (protons), C^e_{ul} ($C^{\rm H}_{ul}$) is the collisional de-excitation rate for collision with e^- (protons), and n_e ($n_{\rm H}$) is the number density of e^- (protons). For the [C II] 158 μm line emission $A_{ul} = 2.36 \times 10^{-6}\,{\rm s}^{-1}$, $C^e_{lu}(T) = (8.63 \times 10^{-6}/g_l\sqrt{T})\,\gamma_{lu}(T)e^{-T_*/T}$, with $\gamma_{lu}(T) \approx 1.6$ if $100 < T < 10^3$ (Gong

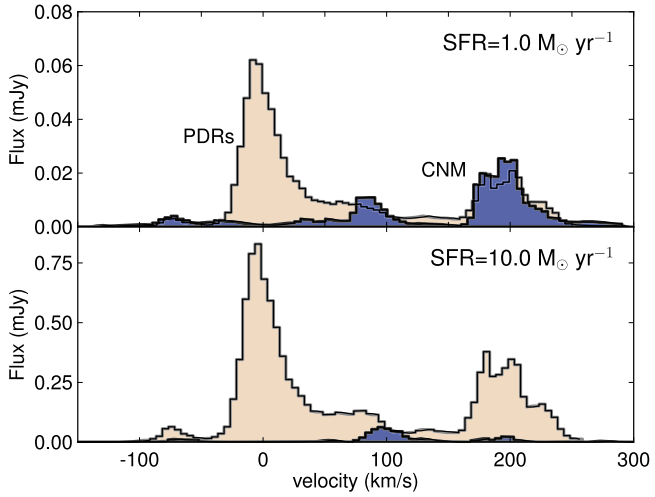

Figure 3. [C II] spectrum for the P005 model assuming SFR $=1\,M_{\odot}\,\mathrm{yr}^{-1}$ (upper panel) and SFR $=10\,M_{\odot}\,\mathrm{yr}^{-1}$ (lower panel) and rebinned over 5 km s^{-1} velocity channels. The emission from PDRs (diffuse neutral medium) is plotted in light red (dark blue).

et al. 2012), $C_{lu}^{\rm H}(T)$ is tabulated in Dalgarno & McCray (1972), and $T_{*}\equiv h\nu_{ul}/k_b\approx 91$ K.

In LTE the collisional excitation and de-excitation rates are related by the following expression that depends on the kinetic temperature T:

$$C_{lu}^{e,\rm H}=\frac{g_u}{g_l}e^{-(T_*/T)}C_{ul}^{e,\rm H}. \quad (6)$$

By combining Equations (5) and (6) we obtain

$$\frac{T_*}{T_{\rm s}}=\ln\frac{A_{ul}\left(1+\frac{c^2I_\nu}{2h\nu^3}\right)+n_eC_{ul}^{e}+n_{\rm H}C_{ul}^{\rm H}}{A_{ul}\left(\frac{c^2I_\nu}{2\,h\nu^3}\right)+n_eC_{ul}^{e}e^{-\frac{T_*}{T}}+n_{\rm H}C_{ul}^{\rm H}e^{-\frac{T_*}{T}}}. \quad (7)$$

As discussed by Gong et al. (2012), the soft UV background at 1330 Å ($I_{\rm UV}$) produced by stars can in principle pump the [C II] ions from the energy level $^2P_{1/2}$ to $^2D_{3/2}$. This pumping effect can lead to the [C II] fin- structure transition $^2D_{3/2}\rightarrow{}^2P_{3/2}\rightarrow{}^2P_{1/2}$, which would mix the levels of the [C II] 158 μm line and thus modify Equation (7). However, the UV pumping effects are negligible in our calculations since the UV intensity inside the galaxy for all of the SFR values considered is much smaller than the critical value for this effect to become important, namely 10^{-15} erg s^{-1} cm^{-2} Hz^{-1} sr^{-1} (Gong et al. 2012).

We calculate the spin temperature of the [C II] transition in the PDRs by substituting into Equation (7) n_e, $n_{\rm H}$, and T as found from the UCL_PDR outputs. The gas temperature within PDRs depends on the radius considered and on the SFR and ranges between $20.7<\langle T\rangle<800$ K. We find that $T_s^{\rm PDR}\sim 30-120$ K for SFR $=0.1$–$100\,M_{\odot}\,\mathrm{yr}^{-1}$. The T_s in the CNM is calculated by considering the n_e, $n_{\rm H}$, and T_k provided by the V13 sub-grid model. We obtain $T_s^{\rm CNM}\sim$ 22–23 K, approximately constant in the range of SFRs considered.

Since at $z\approx 6.6\,T_{\rm CMB}\approx 20.7$ K, we find that the [C II] emission arising from PDRs is only slightly affected by the CMB ($\zeta\approx 0.8$–1.0). Vice versa, the CNM is strongly attenuated at this redshift ($\zeta\approx 0.1$–0.2); in this case the CMB effect becomes negligible only for galaxies at $z\leqslant 4.5$.

3. RESULTS

In Figure 3, we show the [C II] spectrum obtained from the P005 model, assuming SFR $=1\,M_{\odot}\,\mathrm{yr}^{-1}$ (top panel) and SFR $=10\,M_{\odot}\,\mathrm{yr}^{-1}$ (bottom panel). In this figure, the contributions to the [C II] emission arising from PDRs and the CNM are shown in light red and dark blue, respectively.

The emission from PDRs arises predominantly from the center of the galaxy, covering the velocity channels around $\sim$0 km s^{-1}. The second peak in the PDR emission at $v\sim 200$ km s^{-1} is produced by MCs located in the CNM clumps at the periphery of the galaxy (see Figure 2). [C II] emission from the diffuse medium, visible as the two peaks around $\sim$100 and $\sim$200 km s^{-1} is instead always displaced from the center of the galaxy. The [C II] line is relatively narrow, with a FWHM $\sim$ 50 km s^{-1}, as in V13. In Figure 4, we plot the relative contribution of the diffuse medium to the total [C II] emission, $F_{\rm diff}/F_{\rm tot}$, as a function of the SFR, for different C- and P-models, taking into account the CMB attenuation (dark blue). We find that the [C II] emission in $z\approx 6$ galaxies is dominated by PDRs, since the CNM contribution is always $\leqslant$10%, regardless of the metallicity profile and SFR considered.

When the CMB attenuation of the CNM luminosity is negligible (i.e., typically for sources located at $z\leqslant 4.5$; see Section 2.4), we find $F_{\rm diff}/F_{\rm tot}=0.05$–0.45 (cf. Table 1), consistent with several observations of [C II] emission in nearby galaxies (Cormier et al. 2012; Kramer et al. 2013; Parkin et al. 2013; Langer et al. 2014).

3.1. The [C II]–SFR Relation

In the previous section, we found that the [C II] emission is dominated by PDRs, implying $L_{\rm CII}\propto M_{\rm H_2}$. We rescale the [C II] luminosity of our "fiducial" model (SFR $=10\,M_{\odot}\,\mathrm{yr}^{-1}$, $M_{\rm H_2}=4\times10^8 M_{\odot}$) to an arbitrary molecular content by assuming the Kennicutt–Schmidt (KS) relation (Kennicutt et al. 1998; Kennicutt & Evans 2012), namely a power-law correlation between the SFR and molecular gas surface densities, $\Sigma_{\rm SFR}\propto\Sigma_{\rm H_2}^N$. The range in power-law index (N) relating $\Sigma_{\rm SFR}$ and $\Sigma_{\rm H_2}$ depends on a variety of factors, among which the most important ones are the observed scale and the calibration of SFRs. Kennicutt et al. (1998) and Narayanan et al. (2012) report super-linear indices $N=1.4$ and $N\approx 2$, respectively, while Bigiel et al. (2008) inferred an approximately linear molecular KS relation. More recently Shetty et al. (2013), by performing a hierarchical Bayesian analysis on the same sample considered by Bigiel et al. (2008), conclude that $N=0.84$, with a 2σ range [0.63–1.0]. In what follows we scale the molecular mass with the SFR by adopting $N=1$, leaving our discussion on the impact of different N on the [C II]–SFR relation to the last section.

In Figure 5, we show the result of this procedure for different metallicity profiles. Models with uniform metallicity are shown with a black dotted line for $Z=Z_{\odot}$ (C1), an orange solid line for $Z=0.2\,Z_{\odot}$ (C02), and a blue dot–dashed line for $Z=0.05\,Z_{\odot}$ (C005). The results from our C-models are well-described by the following best-fitting formula:

$$\log L_{\rm CII}=7.0+1.2\ \log(\mathrm{SFR})+0.021\ \log(Z)+0.012\ \log(\mathrm{SFR})\log(Z)-0.74\ \log^2(Z), \quad (8)$$

where $L_{\rm CII}$ is expressed in solar units, and the SFR is expressed in $M_{\odot}\,\mathrm{yr}^{-1}$. The magenta dashed line indicates the predictions for the Z–Δ relation with $\langle Z\rangle=0.05Z_{\odot}$ (P005). The slope of

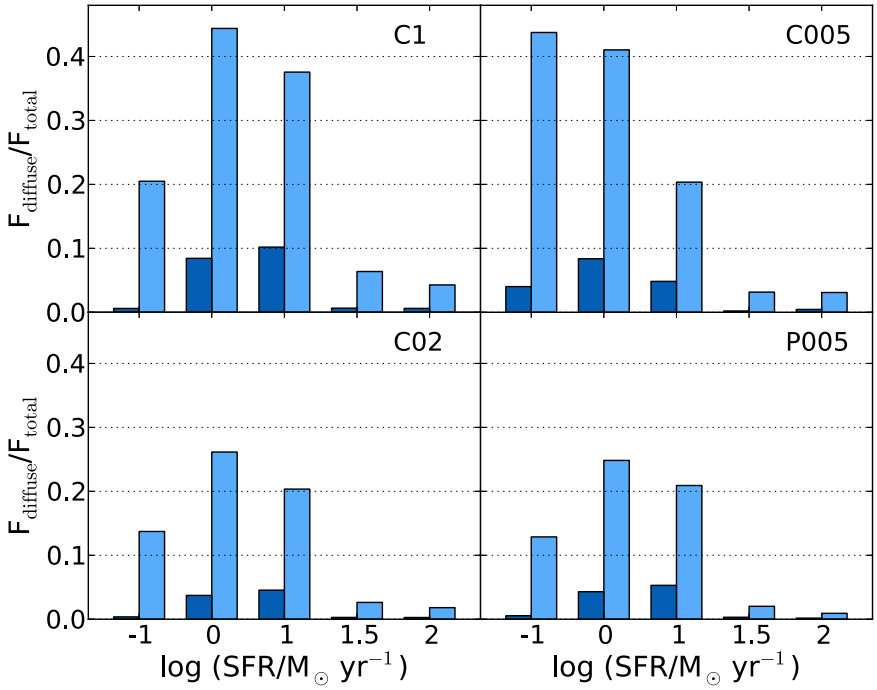

Figure 4. Fraction of the [C II] flux arising from the diffuse medium (F_{diff}) over the total flux (F_{tot}), for four different models, as a function of the SFR, with (dark blue) and without (light blue) taking into account the CMB effects on the [C II] emission.

Table 1
Summary of the Models Considered and Relative Results

			F_{diff}/F_{tot} (%)			L_{CII} ($10^8\,L_\odot$)		
Name	$\langle\frac{Z}{Z_\odot}\rangle$	Profile	1 $M_\odot$ yr^{-1}	10 $M_\odot$ yr^{-1}	100 $M_\odot$ yr^{-1}	1 $M_\odot$ yr^{-1}	10 $M_\odot$ yr^{-1}	100 $M_\odot$ yr^{-1}
C1	1	cnst	44(**8**)	37(**10**)	4(**0.6**)	0.1	1.6	21
C02	0.2	cnst	26(**4**)	20(**5**)	2(**0.2**)	0.05	0.7	9.0
C005	0.05	cnst	41(**8**)	20(**5**)	3(**0.2**)	0.007	0.09	1
P005	0.05	Δ–Z	24(**4**)	21(**5**)	2(**0.3**)	0.05	0.6	8.0

Notes. Name: model name, $\langle Z/Z_\odot\rangle$: mean metallicity in solar units, profile: type of metallicity profile adopted, F_{diff}/F_{tot}: percentage of the [C II] emission arising from the CNM without (and with, in bold) the attenuation due to the increased CMB temperature, L_{CII}: predicted [C II] luminosity in $10^8\,L_\odot$.

the [C II]–SFR relation does not depend either on $\langle Z\rangle$ or on the metallicity distribution. Moreover, the [C II] luminosity predicted by the P005 model is almost coincident with that obtained from the C02 model, in the entire range of SFRs considered. This can be understood by considering that in the case of a overdensity-dependent metallicity profile the PDRs located at the center and dominating the emission have $Z_{PDR} > \langle Z\rangle$, and more precisely, $Z_{PDR} \approx 0.2\,Z_\odot$, namely the metallicity value of the C02 model.

We compare our predictions with the [C II]–SFR relations and their 1σ scatter found by De Looze et al. (2014) for local dwarf galaxies (dark gray shaded region) and local starburst galaxies (light gray shaded region). Dwarf galaxy data by De Looze et al. (2014) are shown through filled circles, individually color-coded according to their Z. Upper limits on the [C II] luminosity from $z \approx 6$–7 LAEs and LBGs data are indicated with empty symbols (Ouchi et al. 2013; González-López et al. 2014; Ota et al. 2014; Maiolino et al. 2015; Schaerer et al. 2015). The recent [C II] detection in the vicinity of a $z \approx 7.1$ LAE (Maiolino et al. 2015) is plotted as a filled square, while [C II] data at $z \approx 5$–6 by Capak et al. (2015) and Willott et al. (2015) are indicated with filled hexagons and triangles, respectively. The [C II]–SFR relation predicted by our model fairly reproduces the slope of the relation found in local dwarfs, as well as its trend with metallicity, although the scatter in the data is large. As shown in Figure 5, the [C II] emission arising from the diffuse medium is expected to be $\leqslant$40% in local galaxies, where the CMB attenuation on the CNM luminosity is negligible. This implies that the [C II]–SFR relation is always driven by the correlation between the SFR and the intensity of the [C II] emission arising from PDRs, with and without taking into account CMB effects. Possible variations in the diffuse medium contribution to the total [C II] emission may result in a slight tilt of the [C II]–SFR relation, certainly within the current 1σ scatter.

4. SUMMARY AND DISCUSSION

By coupling RT cosmological simulations of a $z = 6.6$ galaxy with a sub-grid ISM model and a PDR code (`UCL_PDR`), we have computed the [C II] emission arising

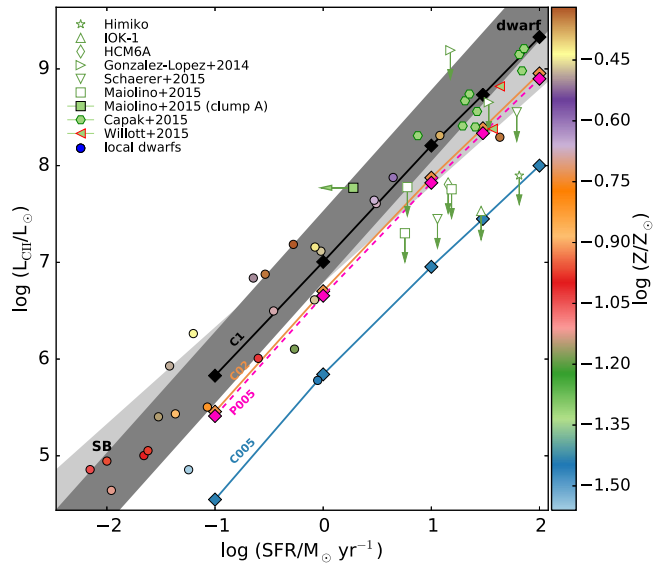

Figure 5. [C II] luminosities in solar units as a function of the SFR. Results from this work are shown with big diamonds and lines color-coded as a function of the metallicity. Solid lines represent the result obtained assuming a constant metallicity: black for $Z = Z_{\odot}$ (C1), orange for $Z = 0.2\,Z_{\odot}$ (C02), and blue for $Z = 0.05\,Z_{\odot}$ (C005). The magenta dashed line corresponds to a density-dependent metallicity (see Section 2.2) with $\langle Z \rangle = 0.05\,Z_{\odot}$ (P005). Model predictions are compared with the data of local dwarf galaxies individually denoted by circles that are color-coded according to their metallicity (De Looze et al. 2014). The 1σ scatters around the best-fit relation for dwarf and local starburst galaxies are plotted in dark gray and light gray, respectively. The green empty (filled) points represent upper limits (detections) of [C II] in LAEs and LBGs at $z \approx 5$–7. More precisely, the filled square represents the [C II] detection nearby BDF3299. as reported by Maiolino et al. (2015), th4 filled hexagons show recent observations by Capak et al. (2015), and the filled triangles with red edges denote data by Willott et al. (2015). Upper limits on BDF3299, BDF512, and SDF46 Maiolino et al. (2015) are plotted with empty squares, along with the upper limits on Himiko (Ouchi et al. 2013; Ota et al. 2014; empty star), IOK-1 (Ota et al. 2014; up-triangle), HCM6A (Kanekar et al. 2013; empty diamond), A1703-zD1, and z8-GND-5296 (Schaerer et al. 2015; empty down-triangle), and SDF1543 and SDF3058 (González-López et al. 2014; empty left triangle).

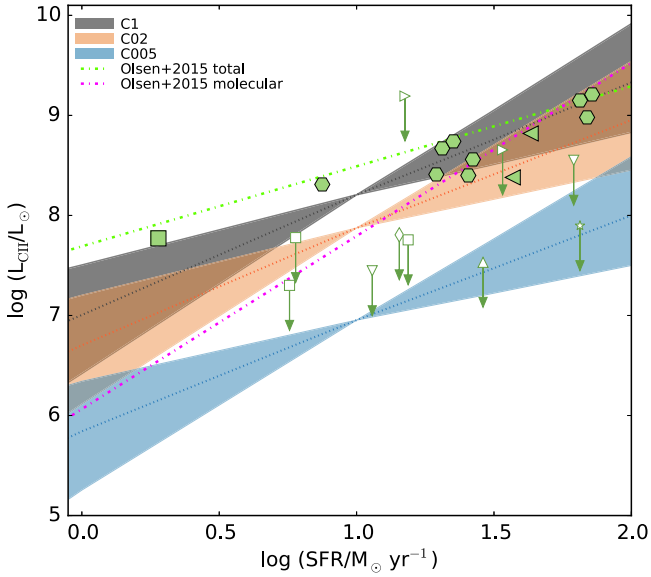

Figure 6. [C II]–SFR relation for the C1, C02, and C005 models as a function of the slope (N) of the KS relation, with N ranging from 0.63 to 2.0. We indicate with thin dotted lines the [C II]–SFR relation obtained for our fiducial model with ($N = 1$). The [C II] luminosity arising from all gas phases, and only from the molecular phase predicted by Olsen et al. (2015), for a sample of $z \approx 2$ galaxies with metallicities ranging from $0.4\,Z_{\odot}$ to $1.67\,Z_{\odot}$, are plotted with green (purple) dot–dashed lines, respectively. The green empty (filled) points represent upper limits (detections) of [C II] in LAEs and LBGs at $z \approx 5$–7, as in Figure 5.

from the diffuse CNM and MCs in early galaxies, characterized by SFRs ranging from 0.1 to $100\,M_{\odot}\,\mathrm{yr}^{-1}$. We have distributed metals in the ISM, both uniformly and according to the Z–Δ relation found by Pallottini et al. (2014a), to simulate gas metallicities in the range 0.05–1 $Z_{\odot}$.

We find that the [C II] line from high-z galaxies is dominated by emission from PDRs, while the CNM accounts for $\leqslant$10% of the total flux. This is due to the fact that at these early epochs the CMB temperature approaches the spin temperature of the [C II] transition in the CNM ($T_{\rm CMB} \sim T_s^{\rm CNM} \sim 20$ K) suppressing the flux contrast. The [C II] spectrum predicted by our model is complex. It shows a pronounced peak (FWHM $\sim$ $50\,\mathrm{km\,s}^{-1}$) due to centrally located ($v = 0$) PDRs, and weaker [C II] displaced ($v \sim 200\,\mathrm{km\,s}^{-1}$) peaks from MCs in the galaxy outskirts.

The predicted [C II]–SFR relation reproduces the corresponding relation found in local dwarfs remarkably well. Current upper limits from observations of $z \sim 6$–7 LAEs and LBGs seem to indicate that these galaxies are characterized by a [C II] luminosity fainter than expected from the local relation. Although this conclusion is still not definitive, it must be noted that the SFRs quoted for high-z galaxies are inferred from observations of the Lyα emission line, and therefore must be considered to be lower limits to the actual value. This implies that the green arrows in Figure 5 should be moved toward higher SFR values, hence exacerbating the inconsistency with the local relation.

Our results contain a caveat: so far we have neglected the possible effect of stellar feedback (i.e., photo-evaporation, radiation pressure, [H II] thermal pressure) on MCs. Broadly speaking, these effects should act to reduce the mass of the molecular gas (Tasker & Tan 2009; Tasker 2011; Tasker et al. 2015). On the other hand, the expansion of [H II] regions might have either a positive effect, by triggering new SF (e.g., Mellema et al. 2006; Bisbas et al. 2011; Haworth & Harries 2012), or disperse the surrounding cloud (Dale et al. 2005). Typical negative feedback timescales range from 1 to 10 Myr (Krumholz et al. 2006; Walch et al. 2012), namely the age of stars taken into account in our RT calculations. This would imply a steeper scaling between the SFR and molecular hydrogen surface densities,because for a given value of SFR, the mass of H_2 is lower.

In Figure 6 we plot the [C II]–SFR relation for models with constant metallicity (C1, C02, and C005) as a function of the slope in the range $0.63 \leqslant N \leqslant 2.0$ (Bigiel et al. 2008; Narayanan et al. 2012; Shetty et al. 2013). For reference we show the [C II]–SFR relation obtained for our fiducial model $N = 1$ with thin dotted lines. At a given Z the steeper the slope of the KS relation, the shallower the [C II]–SFR curve. Hence, a [C II] deficit in $z \sim 6$–7 galaxies, if confirmed by deeper observations, would favor a scenario in which SF in early galaxies blows the molecular gas apart, reducing the amount of material from which most of the [C II] emission arises. The deviation from the local [C II]–SFR would then imply a modified KS relation in $z > 6$ galaxies. Stellar feedback effects are likely to be stronger in regions of very active SF, which are more often located in galactic centers. This is particularly important in high-z galaxies that are known to be more compact

than their low-z counterparts. If so, negative feedback should preferentially suppress the peak in the [C II] spectrum at the systemic redshift of the galaxy. Alternatively/in addition, as can be noted in Figure 6, the deficit might be explained by lower gas metallicities.

In the same figure, we also test our results with the [C II]–SFR relation for all gas phases (PDR + molecular + ionized) and only from the molecular phase, as calculated by Olsen et al. (2015) in a sample of simulated $z \approx 2$ galaxies. As they point out in their work, their PDR component is best identified with what we call CNM, while their molecular component, located at the center, is comparable to what we call PDR emission. We find a nice agreement between our results and their findings for the molecular gas. This is somewhat expected, given that the fraction of [C II] emission arising from the CNM is almost totally attenuated due to the increased CMB temperature at $z \approx 6.6$.

Finally, we note that the MC density distribution may play a role. Our simulated galaxy is characterized by a mean molecular hydrogen number density $n_{\rm cl} \sim 10^{2.9}\,{\rm cm}^{-3}$; this quantity depends on the square of the assumed Mach number $\mathcal{M} = 10$. Calculations performed with UCL_PDR show that MCs characterized by densities 10 times higher (lower), for a fixed gas metallicity (e.g., $\log(Z/Z_{\odot}) = -1.5$), would result in a [C II] emissivity that is five times higher (20 times lower) than found here. Although we consider such large variations of the Mach number unlikely, at present we cannot exclude that the corresponding shift in the mean MC density plays some role in the interpretation of the results.

REFERENCES

Bayet, E., Gerin, M., Phillips, T. G., & Contursi, A. 2009, MNRAS, 399, 264
Bell, T. A., Viti, S., & Williams, D. A. 2007, MNRAS, 378, 983
Bell, T. A., Viti, S., Williams, D. A., Crawford, I. A., & Price, R. J. 2005, MNRAS, 357, 961
Bigiel, F., Leroy, A., Walter, F., et al. 2008, AJ, 136, 2846
Bisbas, T. G., Wünsch, R., Whitworth, A. P., Hubber, D. A., & Walch, S. 2011, ApJ, 736, 142
Boselli, A., Gavazzi, G., Lequeux, J., & Pierini, D. 2002, A&A, 385, 454
Bouwens, R. J., Illingworth, G. D., Oesch, P. A., et al. 2012, ApJ, 754, 83
Capak, P. L., Carilli, C., Jones, G., et al. 2015, Natur, 522, 455
Carilli, C. L., Riechers, D., Walter, F., et al. 2013, ApJ, 763, 120
Carilli, C. L., & Walter, F. 2013, ARA&A, 51, 105
Carniani, S., Marconi, A., Biggs, A., et al. 2013, A&A, 559, A29
Cicone, C., Maiolino, R., Gallerani, S., et al. 2015, A&A, 574, A14
Cormier, D., Lebouteiller, V., Madden, S. C., et al. 2012, A&A, 548, A20
Cox, P., Krips, M., Neri, R., et al. 2011, ApJ, 740, 63
da Cunha, E., Groves, B., Walter, F., et al. 2013, ApJ, 766, 13
Dale, J. E., Bonnell, I. A., Clarke, C. J., & Bate, M. R. 2005, MNRAS, 358, 291
Dalgarno, A., & McCray, R. A. 1972, ARA&A, 10, 375
De Breuck, C., Williams, R. J., Swinbank, M., et al. 2014, A&A, 565, A59
De Looze, I., Baes, M., Bendo, G. J., Cortese, L., & Fritz, J. 2011, MNRAS, 416, 2712
De Looze, I., Cormier, D., Lebouteiller, V., et al. 2014, A&A, 568, A62
Gallerani, S., Neri, R., Maiolino, R., et al. 2012, A&A, 543, A114
Gong, Y., Cooray, A., Silva, M., et al. 2012, ApJ, 745, 49
González, V., Labbé, I., Bouwens, R. J., et al. 2011, ApJL, 735, L34
González-López, J., Riechers, D. A., Decarli, R., et al. 2014, ApJ, 784, 99
Haworth, T. J., & Harries, T. J. 2012, MNRAS, 420, 562
Hennebelle, P., & Chabrier, G. 2011, ApJL, 743, L29
Hennebelle, P., & Chabrier, G. 2013, ApJ, 770, 150
Herrera-Camus, R., Bolatto, A. D., Wolfire, M. G., et al. 2015, ApJ, 800, 1
Hollenbach, D. J., & Tielens, A. G. G. M. 1999, RvMP, 71, 173
Kainulainen, J., & Tan, J. C. 2013, A&A, 549, A53
Kanekar, N., Wagg, J., Ram Chary, R., & Carilli, C. L. 2013, ApJL, 771, L20
Kapala, M. J., Sandstrom, K., Groves, B., et al. 2015, ApJ, 798, 24
Keating, L. C., Haehnelt, M. G., Becker, G. D., & Bolton, J. S. 2014, MNRAS, 438, 1820
Kennicutt, R. C., & Evans, N. J. 2012, ARA&A, 50, 531
Kennicutt, R. C., Jr., Stetson, P. B., Saha, A., et al. 1998, ApJ, 498, 181
Kim, W.-T., & Ostriker, E. C. 2002, ApJ, 570, 132
Kim, W.-T., Ostriker, E. C., & Stone, J. M. 2003, ApJ, 599, 1157
Kramer, C., Abreu-Vicente, J., García-Burillo, S., et al. 2013, A&A, 553, A114
Krumholz, M. R., Matzner, C. D., & McKee, C. F. 2006, ApJ, 653, 361
Krumholz, M. R., & McKee, C. F. 2005, ApJ, 630, 250
Langer, W. D., Pineda, J. L., & Velusamy, T. 2014, A&A, 564, A101
Leitherer, C., Schaerer, D., Goldader, J. D., et al. 1999, ApJS, 123, 3
Maiolino, R., Carniani, S., Fontana, A., et al. 2015, MNRAS, 452, 54
Maiolino, R., Cox, P., Caselli, P., et al. 2005, A&A, 440, L51
Mellema, G., Arthur, S. J., Henney, W. J., Iliev, I. T., & Shapiro, P. R. 2006, ApJ, 647, 397
Muñoz, J. A., & Furlanetto, S. R. 2014, MNRAS, 438, 2483
Murray, N. 2011, ApJ, 729, 133
Nagamine, K., Wolfe, A. M., & Hernquist, L. 2006, ApJ, 647, 60
Narayanan, D., Krumholz, M. R., Ostriker, E. C., & Hernquist, L. 2012, MNRAS, 421, 3127
Olsen, K. P., Greve, T. R., Narayanan, D., et al. 2015, arXiv:1507.00362
Ostriker, E. C., Stone, J. M., & Gammie, C. F. 2001, ApJ, 546, 980
Ota, K., Walter, F., Ohta, K., et al. 2014, ApJ, 792, 34
Ouchi, M., Ellis, R., Ono, Y., et al. 2013, ApJ, 778, 102
Ouchi, M., Ono, Y., Egami, E., et al. 2009, ApJ, 696, 1164
Padoan, P. 1995, MNRAS, 277, 377
Padoan, P., Federrath, C., Chabrier, G., et al. 2014, in Protostars and Planets VI, ed. H. Beuther et al. (Tucson, AZ: Univ. Arizona Press), 77
Padoan, P., & Nordlund, Å. 2011, ApJ, 730, 40
Pallottini, A., Ferrara, A., Gallerani, S., Salvadori, S., & D'Odorico, V. 2014a, MNRAS, 440, 2498
Pallottini, A., Gallerani, S., & Ferrara, A. 2014b, MNRAS, 444, L105
Papadopoulos, P. P. 2010, ApJ, 720, 226
Parkin, T. J., Wilson, C. D., Schirm, M. R. P., et al. 2013, ApJ, 776, 65
Pineda, J. L., Langer, W. D., & Goldsmith, P. F. 2014, A&A, 570, A121
Pineda, J. L., Langer, W. D., Velusamy, T., & Goldsmith, P. F. 2013, A&A, 554, A103
Popping, G., Pérez-Beaupuits, J. P., Spaans, M., Trager, S. C., & Somerville, R. S. 2014, MNRAS, 444, 1301
Riechers, D. A., Carilli, C. L., Capak, P. L., et al. 2014, ApJ, 796, 84
Sargsyan, L., Lebouteiller, V., Weedman, D., et al. 2012, ApJ, 755, 171
Schaerer, D., Boone, F., Zamojski, M., et al. 2015, A&A, 574, A19
Shetty, R., Kelly, B. C., & Bigiel, F. 2013, MNRAS, 430, 288
Springel, V. 2005, MNRAS, 364, 1105
Stacey, G. J., Geis, N., Genzel, R., et al. 1991, ApJ, 373, 423
Tasker, E. J. 2011, ApJ, 730, 11
Tasker, E. J., & Tan, J. C. 2009, ApJ, 700, 358
Tasker, E. J., Wadsley, J., & Pudritz, R. 2015, ApJ, 801, 33
Teyssier, R. 2002, A&A, 385, 337
Tielens, A. G. G. M., & Hollenbach, D. 1985, ApJ, 291, 722
Vallini, L., Dayal, P., & Ferrara, A. 2012, MNRAS, 421, 3266
Vallini, L., Gallerani, S., Ferrara, A., & Baek, S. 2013, MNRAS, 433, 1567
Vazquez-Semadeni, E. 1994, ApJ, 423, 681
Venemans, B. P., McMahon, R. G., Walter, F., et al. 2012, ApJL, 751, L25
Wada, K. 2008, ApJ, 675, 188
Wagg, J., Kanekar, N., & Carilli, C. L. 2009, ApJL, 697, L33
Walch, S. K., Whitworth, A. P., Bisbas, T., Wünsch, R., & Hubber, D. 2012, MNRAS, 427, 625
Walter, F., Decarli, R., Carilli, C., et al. 2012, ApJ, 752, 93
Williams, R. J., Wagg, J., Maiolino, R., et al. 2014, MNRAS, 439, 2096
Willott, C. J., Carilli, C. L., Wagg, J., & Wang, R. 2015, ApJ, 807, 180
Wolfire, M. G., Hollenbach, D., McKee, C. F., Tielens, A. G. G. M., & Bakes, E. L. O. 1995, ApJ, 443, 152
Wolfire, M. G., McKee, C. F., Hollenbach, D., & Tielens, A. G. G. M. 2003, ApJ, 587, 278
Zabl, J., Nørgaard-Nielsen, H. U., Fynbo, J. P. U., et al. 2015, MNRAS, 451, 2050
Zheng, W., Postman, M., Zitrin, A., et al. 2012, Natur, 489, 406